Scientific Open Access Publishing

Simen Owen Academic Proceedings Series

4th International Conference on Education, Environment, Arts and Social Science (EESD 2026)

Article

Spatiotemporal Variation of Vegetation Greenness and Its Climate Response in the Da Hinggan Mountains

Zhichu Zhang[1,*]

[1] Northeast Forestry University, Harbin, China
* Correspondence: Zhichu Zhang, Northeast Forestry University, Harbin, China

Abstract: Understanding vegetation greenness dynamics and their climatic drivers in cold-temperate forest ecosystems is essential for regional ecological assessment and sustainable forest management. This study investigated the spatiotemporal characteristics of vegetation greenness and its response to climate variability in the Da Hinggan Mountains, a critical cold-temperate forest region in northeastern China. Using the Google Earth Engine platform, we acquired Landsat-derived growing-season maximum normalized difference vegetation index (NDVI) composites, ERA5-Land temperature and precipitation datasets, and SRTM digital elevation model data spanning 13 biennial growing-season snapshots from 2000 to 2024. The Theil–Sen median slope estimator and Mann–Kendall trend test were employed to detect spatial trends in NDVI, temperature, and precipitation, while partial correlation analysis was applied to quantify the independent linear relationships between climatic variables and NDVI change. Results indicated that the regional mean growing-season maximum NDVI increased from 0.376 in 2000 to 0.404 in 2024, reflecting a gradual overall greening trend. At the pixel scale, significantly greening pixels constituted 22.26% of valid pixels, significantly degrading pixels accounted for 0.97%, and pixels exhibiting non-significant change comprised 76.78%. Meteorological trend analysis revealed predominantly negative temperature slopes without statistically significant warming areas, alongside a widespread but weakly significant increasing precipitation tendency. Partial correlation analysis demonstrated that areas with significant correlations between NDVI and temperature or precipitation were limited to 2.57% and 3.92%, respectively, while 94.12% of the region lacked significant climate response. These findings suggest that vegetation greenness changes in the Da Hinggan Mountains result from the combined influence of forest natural succession, ecological conservation policies, topographic factors, and nonlinear climate interactions, rather than linear climatic forcing alone.

Keywords: vegetation greenness; ndvi; climate response; cold-temperate forest; trend analysis

Received: 07 July 2026
Revised: 19 August 2026
Accepted: 01 September 2026
Published: 04 September 2026

1. Introduction

Forest ecosystems constitute a foundational component of regional ecological security, exerting critical influence on hydrological regulation, energy balance, and carbon sequestration within the terrestrial biosphere. High-latitude and cold-temperate forests exhibit heightened responsiveness to climatic perturbations due to their narrow thermal tolerance windows, slow decomposition rates, and strong coupling between snowmelt dynamics, soil freeze-thaw cycles, and phenological development. Vegetation greenness—quantified as the integrated spectral response of photosynthetically active vegetation—is a robust integrative indicator of ecosystem vitality, physiological activity, and structural integrity. Changes in greenness patterns across time and space not only reflect shifts in species composition, canopy density, and leaf area index but also encode information about underlying biophysical drivers such as moisture availability, growing season length, and disturbance recovery trajectories. The Da Hinggan Mountains, situated in northeastern China's cold-temperate forest biome, function as a vital ecological buffer zone that mitigates dust transport, stabilizes regional water cycles, and supports biodiversity conservation across northern Eurasia. Its steep latitudinal gradient—from boreal transition zones near the Russian border to mixed conifer–broadleaf ecotones further south—combined with marked elevational zonation and heterogeneous hydrothermal regimes, renders this region an exemplary natural laboratory for investigating vegetation–climate feedbacks under ongoing global change.

The Normalized Difference Vegetation Index (NDVI) remains one of the most widely adopted optical remote sensing indices for characterizing vegetation greenness at regional to continental scales. Derived from the differential reflectance in the red and near-infrared spectral bands, NDVI provides a dimensionless, normalized measure sensitive to chlorophyll content, canopy structure, and leaf water status. While NDVI correlates strongly with vegetation vigor and fractional cover under many conditions, it is essential to recognize its inherent limitations: it does not directly quantify forest canopy closure, nor does it distinguish between tree species, understory contribution, or non-photosynthetic vegetation elements. Moreover, atmospheric scattering, soil background effects, and sensor calibration differences can introduce systematic biases, particularly in sparse or heterogeneous canopies [1]. Therefore, this study explicitly adopts NDVI as an operational proxy for integrated vegetation greenness and surface cover condition, interpreting temporal trends and spatial patterns strictly within the context of spectral response rather than as direct surrogates for structural forest metrics such as crown closure or basal area.

Vegetation dynamics in the Da Hinggan Mountains emerge from the complex interplay of multiple abiotic and biotic factors operating across distinct spatial and temporal scales. Climatic variables—including mean annual temperature, seasonal precipitation distribution, frost-free period duration, and extreme event frequency—interact nonlinearly with topographic attributes such as slope, aspect, elevation, and terrain curvature to shape microclimatic niches and edaphic conditions. Stand-level characteristics—including age structure, dominant species composition, and post-disturbance regeneration history—further modulate local greenness responses. In parallel, long-term conservation initiatives—including natural forest protection programs, reforestation campaigns, and grazing restrictions—have introduced anthropogenic signals into vegetation trajectories that may either amplify or counteract climate-driven trends [2]. Given this multifactorial control architecture, isolating the relative contributions of individual drivers requires rigorous statistical treatment: consistent temporal coverage of high-resolution NDVI time series must be paired with homogenized meteorological records, harmonized digital elevation models, and spatially explicit land management histories—all analyzed within a unified geospatial framework that accounts for autocorrelation, scale mismatch, and nonstationarity in vegetation–climate relationships.

2. Data Sources

2.1. NDVI Data

NDVI data were derived from the Landsat surface reflectance product series accessible via the Google Earth Engine platform, ensuring consistent radiometric calibration and atmospheric correction across the entire time series. The study period encompasses twenty-four consecutive years, from 2000 through 2024, with biennial sampling yielding thirteen temporally discrete observations corresponding to the years 2000, 2002, 2004, 2006, 2008, 2010, 2012, 2014, 2016, 2018, 2020, 2022, and 2024. To enhance ecological relevance and signal stability, all satellite scenes were temporally constrained to the local growing season—defined regionally using phenological thresholds based on long-term climatology and vegetation onset metrics [1, 3]. Within each biennial interval, the Maximum Value Composite method was applied to synthesize cloud-free, high-quality pixel values, thereby generating a robust representation of peak seasonal greenness. This compositing strategy effectively minimizes the impact of transient atmospheric conditions, sensor noise, and geometric artifacts without introducing temporal interpolation bias.

Rigorous annual quality assessment confirmed that the proportion of valid, non-masked pixels remained highly stable across all thirteen time steps, averaging approximately 53.48% with negligible interannual fluctuation—indicating consistent data availability and processing reliability throughout the study period [4, 5]. Regional mean NDVI values ranged narrowly between 0.376 and 0.414, reflecting moderate to high vegetation density typical of the study area's dominant land cover types, while the standard deviation remained tightly bounded between 0.050 and 0.056, underscoring spatial homogeneity in vegetation response. No outliers or discontinuities were observed in either central tendency or dispersion metrics, confirming the absence of data acquisition failures, algorithmic anomalies, or uncorrected geolocation errors. Collectively, these quantitative diagnostics demonstrate strong temporal coherence, measurement repeatability, and suitability for rigorous trend detection, change-point analysis, and long-term ecological monitoring applications.

2.2. Meteorological and Topographic Data

Meteorological data were acquired from the ERA5-Land monthly reanalysis dataset, accessed via the Google Earth Engine platform. This dataset provides globally consistent, high-temporal-resolution climate variables derived from a state-of-the-art land-surface model constrained by satellite and in situ observations [6]. For this study, growing-season temperature and precipitation metrics were extracted to align temporally with the 13 biennial NDVI snapshots spanning the analysis period. Specifically, temperature was computed as the arithmetic mean of all monthly values occurring within the defined growing season for each year, while precipitation was aggregated as the cumulative sum over the same seasonal window. The native spatial resolution of ERA5-Land is approximately 9 km, which represents a fundamental limit on the spatial fidelity of the meteorological information. Although the data were reprojected and resampled to conform precisely to the NDVI raster grid and the study-area boundary, such geometric alignment does not enhance the intrinsic spatial resolution; thus, all subsequent climatic interpretations remain subject to the constraints imposed by the original 9 km grid scale.

Topographic data were sourced from the Shuttle Radar Topography Mission (SRTM) digital elevation model at 30-meter spatial resolution, also obtained through the Google Earth Engine platform. From this high-resolution DEM, elevation and aspect—defined as the compass direction that a slope faces—were systematically derived using standard geospatial algorithms. These topographic variables served exclusively for stratified statistical analysis, enabling subgroup comparisons across elevation bands and cardinal orientations to assess potential terrain-mediated influences on vegetation dynamics [1]. Importantly, the DEM was not integrated into any meteorological interpolation framework—for instance, it was not used to downscale or correct coarse-resolution climate data—and it was not applied as a direct conversion factor to transform NDVI values into estimates of forest canopy closure or structural attributes. Its role remained strictly descriptive and analytical rather than predictive or modeling-oriented.

3. Methods

3.1. NDVI Extraction and Quality Control

The Normalized Difference Vegetation Index (NDVI) was calculated from Landsat surface reflectance data using the standard spectral formula NDVI = (NIR − Red) / (NIR + Red), where NIR denotes near-infrared band reflectance and Red denotes red band reflectance. Prior to computation, rigorous pixel-level quality control was implemented on the Google Earth Engine (GEE) platform to exclude clouds, cloud shadows, snow-covered surfaces, and other invalid or saturated pixels based on the Quality Assessment

(QA) bands accompanying each Landsat scene [3]. Subsequently, a growing-season maximum value composite approach was applied to all cloud-free observations acquired between April and October for each of the thirteen study years, resulting in one temporally aggregated NDVI raster per year representing peak vegetation greenness. For each annual composite, spatial statistics—including the proportion of valid pixels across the study area, arithmetic mean NDVI, standard deviation, and selected quantiles (e.g., 10th, 25th, 75th, and 90th percentiles)—were systematically derived to assess temporal consistency, detect potential outliers, and ensure data integrity prior to downstream trend analysis and ecological interpretation.

3.2. Trend Analysis

Spatial trends in the Normalized Difference Vegetation Index (NDVI), near-surface air temperature, and accumulated precipitation were quantified using the non-parametric Theil–Sen median slope estimator, which is robust against outliers and does not assume normality or linearity in the underlying data distribution. Statistical significance of monotonic trends was rigorously evaluated using the Mann–Kendall rank correlation test, with a conventional alpha level of 0.05 adopted to determine whether observed directional changes are unlikely to arise from random variation. Given that the temporal dataset comprises thirteen biennial observations spanning the period from 2000 to 2024, the resulting trend estimates reflect the average rate of change per two-year interval rather than annual increments; this temporal resolution inherently emphasizes longer-term ecological and climatic signals while mitigating short-term interannual noise such as those induced by El Niño–Southern Oscillation events or localized extreme weather anomalies [7, 8].

Pixel-level classification of vegetation dynamics was conducted exclusively on the basis of NDVI trend magnitude and statistical reliability: each valid pixel was assigned to one of three mutually exclusive categories—significant greening, significant degradation, or non-significant change. A pixel was classified as exhibiting significant greening if its Theil–Sen slope estimate for NDVI was both positive and statistically significant at $p < 0.05$; conversely, significant degradation required a negative slope meeting the same significance threshold. All remaining pixels with valid NDVI time series but insufficient evidence to reject the null hypothesis of no trend were conservatively grouped into the non-significant change category, thereby ensuring methodological transparency and minimizing Type I error inflation across the spatial domain.

3.3. Topographic Stratification

The recomputed NDVI Theil–Sen slopes and associated Mann–Kendall statistical significance values were spatially integrated with topographic classifications derived from digital elevation models to enable systematic ecological interpretation across terrain gradients [8]. Specifically, the analysis stratified the study area into six discrete elevation belts—namely, below 300 meters, 300–500 meters, 500–700 meters, 700–900 meters, 900–1100 meters, and 1100 meters and above—and further categorized terrain into flat surfaces and eight cardinal and intercardinal aspect classes (north, northeast, east, southeast, south, southwest, west, northwest). For each resulting topographic stratum, summary statistics included the arithmetic mean and median of the NDVI trend slopes, the interquartile range as a robust measure of dispersion, and the proportional distribution of pixels exhibiting statistically significant greening, statistically significant degradation, and non-significant change at the conventional alpha level.

3.4. Partial Correlation Analysis and Climate Response Classification

To isolate the independent linear relationships between climatic variables and vegetation dynamics, pixel-level partial correlation analysis was conducted to disentangle the distinct influences of temperature and precipitation on NDVI change. Specifically, the partial correlation coefficient between NDVI and mean annual temperature was calculated while statistically controlling for the concurrent variation in annual precipitation; conversely, the partial correlation between NDVI and annual precipitation was estimated while holding temperature constant. This dual-control approach enables the identification of unique, non-redundant associations that are not attributable to collinearity between the two climate drivers. Subsequently, each pixel was assigned to one of four mutually exclusive response categories based on statistical significance thresholds ($p < 0.05$) for both partial correlations: temperature-responsive (significant only for temperature), precipitation-responsive (significant only for precipitation), dual-factor-responsive (significant for both), or no-significant-climate-response (neither significant). This classification reflects empirical statistical associations rather than mechanistic causality or relative driver strength, and therefore does not imply hierarchical dominance or process-based attribution.

4. Spatiotemporal Characteristics of NDVI Change in the Da Hinggan Mountains

4.1. Overall Temporal Trend of NDVI

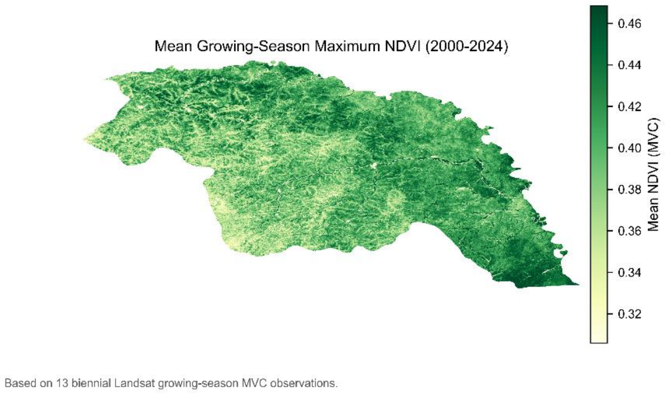

Figure 1. Spatial Distribution of Multi-Year Mean Growing-Season Maximum NDVI in the Da Hinggan Mountains (2000–2024, 13 Biennial Snapshots)

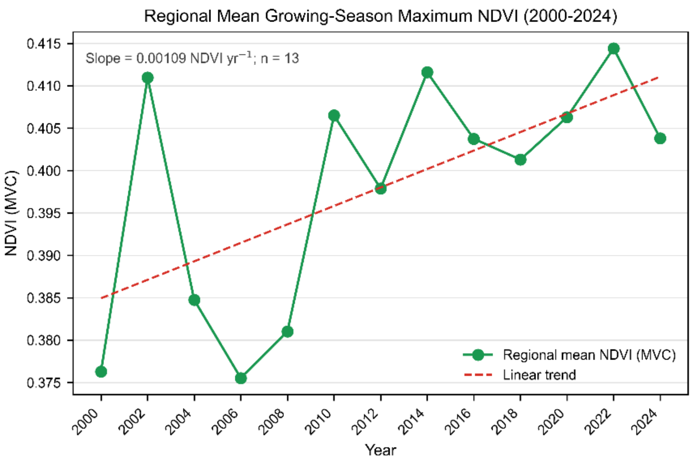

Figure 2. Time Series and Linear Trend of Regional Mean Growing-Season Maximum NDVI in the Da Hinggan Mountains (2000–2024, 13 Biennial Snapshots)

The regional mean growing-season maximum NDVI exhibited a gradual upward trajectory over the 25-year observation period, rising from 0.376 in 2000 to 0.404 in 2024, corresponding to a statistically significant linear trend with a slope of approximately 0.0011 per year. This consistent positive trend reflects a long-term enhancement in vegetation photosynthetic capacity and canopy density across the Da Hinggan Mountains. Interannual variability was evident throughout the time series, with 2006 recording the lowest observed value—likely attributable to transient climatic conditions such as reduced summer precipitation or anomalously cool temperatures during peak growing months—while 2022 registered the highest value, suggesting favorable meteorological and edaphic conditions that supported optimal plant growth. Such fluctuations underscore the responsiveness of vegetation dynamics to natural environmental variability, including seasonal shifts in temperature, moisture availability, and solar radiation, all of which modulate physiological activity and phenological development without implying systemic instability [9] (As shown in Figure 1).

Spatially, the multi-year mean growing-season maximum NDVI displays a clear gradient, increasing progressively from the western and northwestern portions of the region toward the eastern and southeastern sectors. This pattern aligns closely with the underlying topography, hydrology, and soil fertility distribution: the eastern and southeastern subregions are dominated by dense, mature coniferous and mixed forests on relatively moist, nutrient-rich volcanic and brown forest soils, supporting higher leaf area index and chlorophyll concentration; in contrast, the western meadow–forest transition zone features shallower soils, lower water-holding capacity, and greater exposure to continental aridity, resulting in sparser vegetation cover and reduced photosynthetic efficiency. Consequently, pronounced spatial heterogeneity in vegetation greenness is observed—not as an indicator of degradation or imbalance, but as a natural expression of ecological zonation shaped by long-term geomorphic evolution and climate gradients.

4.2. Pixel-Level Trend Analysis

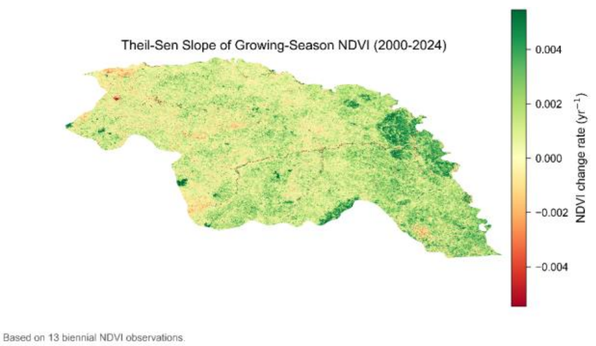

Figure 3. Spatial Distribution of Theil–Sen Slopes of Growing-Season Maximum NDVI in the Da Hinggan Mountains (2000–2024, 13 Biennial Snapshots)

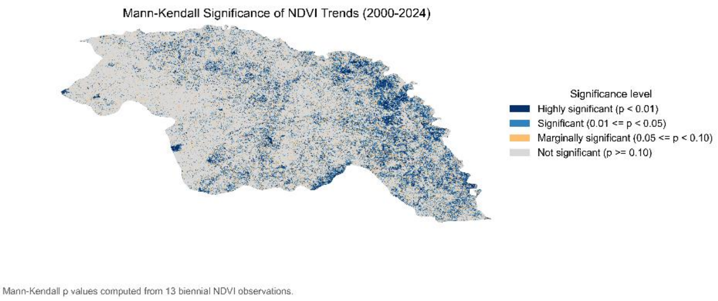

Figure 4. Mann–Kendall Significance Test Results for NDVI Trends in the Da Hinggan Mountains (2000–2024, 13 Biennial Snapshots)

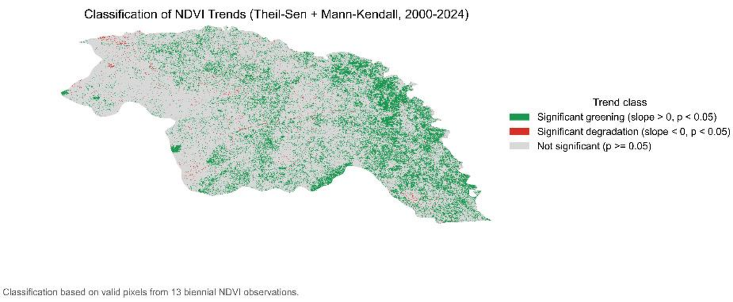

Figure 5. NDVI Trend Classification Map for the Da Hinggan Mountains (Theil–Sen + Mann–Kendall, 2000–2024, 13 Biennial Snapshots)

Recomputed pixel-level statistics across the entire Da Hinggan Mountains region revealed that, out of a total of 115,008,234 valid pixels analyzed, approximately 22.26% exhibited statistically significant greening trends—defined as positive Theil–Sen slopes confirmed by Mann–Kendall test results at $p < 0.05$—while only 0.97% showed statistically significant degradation. The remaining 76.78% of pixels displayed no statistically detectable trend over the 25-year observation period (2000–2024). This distribution indicates that regional vegetation dynamics cannot be accurately summarized by a single directional narrative of uniform greening; instead, the landscape reflects a heterogeneous mosaic where localized strong greening coexists with extensive areas of subtle, non-significant improvement and stable conditions. Such spatial complexity underscores the importance of moving beyond areal averages and adopting high-resolution, pixel-wise analytical frameworks to capture nuanced ecological responses to climate variability, land-use adjustments, and forest management interventions (As shown in Figure 3, 4).

Further decomposition of slope directionality demonstrated that pixels with non-significant positive trends constituted 56.69% of the total valid pixel count, whereas those with non-significant negative trends accounted for 20.09%. This asymmetry strongly suggests an underlying tendency toward vegetation enhancement across much of the study area, even when formal statistical significance is not attained—likely attributable to the relatively short effective temporal baseline (13 biennial snapshots spanning 25 years), combined with pronounced interannual climatic fluctuations and ecosystem inertia. The extremely limited extent of significant degradation—less than 1%—reinforces the conclusion that large-scale vegetation decline has not occurred in this ecologically critical boreal–temperate transition zone. Rather, observed changes appear predominantly driven by gradual, low-magnitude processes such as natural forest succession, post-disturbance recovery, and climate-mediated phenological shifts, all operating within thresholds that maintain overall structural and functional stability of the mountain forest ecosystems.

4.3. NDVI Change Differences Across Topographic Units

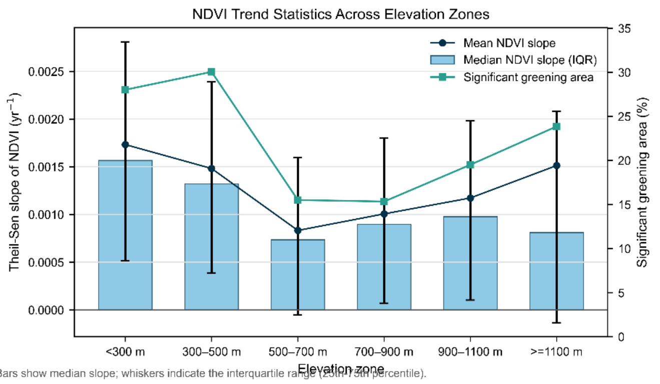

Figure 6. NDVI Trend Statistics by Elevation Belt

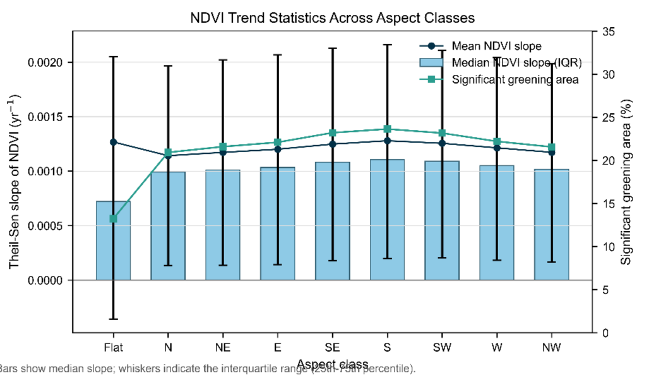

Figure 7. NDVI Trend Statistics by Aspect Class

Topographic stratification revealed that elevation exerts a non-linear modulating influence on NDVI greening trends, contradicting assumptions of monotonic decline with increasing altitude [10]. Specifically, the lowest elevation belts—those below 300 m and between 300–500 m—displayed the strongest positive NDVI trends, with mean annual slopes of 0.001732 a^{-1} and 0.001482 a^{-1}, respectively; these zones also registered the highest proportions of statistically significant greening, at 28.01% and 30.05%. In contrast, the mid-elevation belt (500–900 m) exhibited a marked attenuation in greening intensity, with only approximately 15% of pixels showing significant positive trends. Notably, above 900 m, both the mean NDVI slope and the spatial extent of significant greening increased modestly, suggesting potential ecological thresholds or compensatory responses—such as enhanced snowmelt timing, reduced anthropogenic pressure, or species-specific altitudinal adaptations—that counteract typical climatic constraints at higher elevations. This pattern underscores the importance of incorporating fine-scale topographic heterogeneity into regional vegetation change assessments, particularly in mountainous terrain where microclimatic gradients strongly mediate plant phenology and productivity (As shown in Figure 6).

Aspect-stratified analysis further indicated that all cardinal and intercardinal slope orientations supported net vegetation greening, as reflected by uniformly positive mean NDVI slopes across aspect classes. However, the magnitude of change varied subtly: south-, southeast-, and southwest-facing slopes demonstrated marginally elevated proportions of statistically significant greening, likely attributable to greater solar irradiance, earlier spring thaw, and extended growing seasons under warmer, drier conditions. Conversely, north-facing slopes showed slightly lower greening prevalence, consistent with cooler, moister microclimates that may constrain photosynthetic activity or delay phenological development. Crucially, the inter-aspect differences were quantitatively modest compared to the pronounced elevation-driven divergence, reinforcing the interpretation that aspect functions primarily as a secondary modulating factor—fine-tuning vegetation response within broader altitudinal and climatic envelopes—rather than serving as a dominant control over long-term NDVI trajectories. This hierarchical relationship highlights the need for multi-scale topographic modeling in remote sensing–based ecological monitoring frameworks.

5. Spatiotemporal Characteristics of Meteorological Variables

5.1. Spatial and Temporal Patterns of Temperature

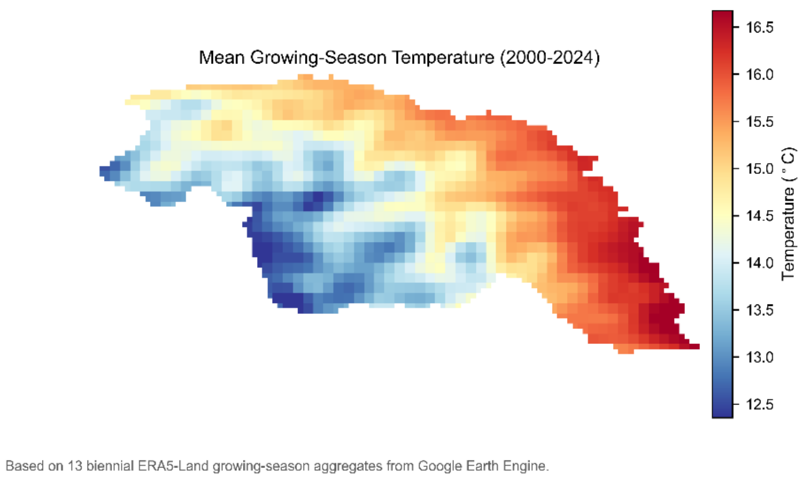

Figure 8. Spatial Distribution of Multi-Year Mean Growing-Season Temperature in the Da Hinggan Mountains (2000–2024, 13 Biennial Snapshots)

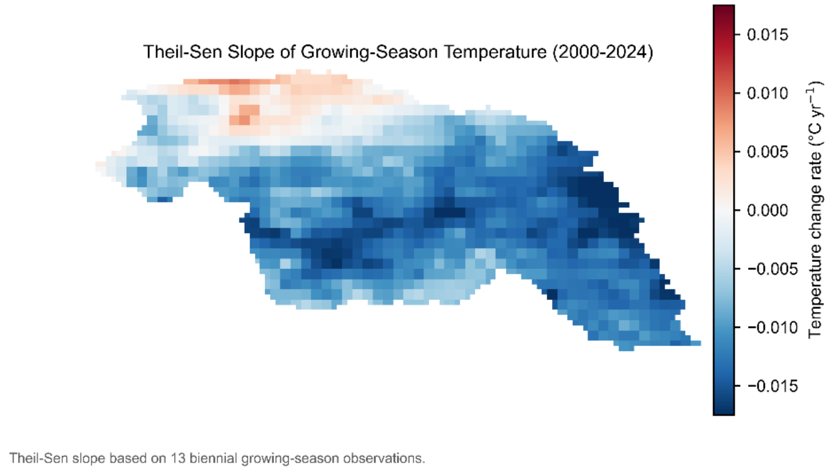

Figure 9. Spatial Distribution of Theil–Sen Slopes of Growing-Season Temperature in the Da Hinggan Mountains (2000–2024, 13 Biennial Snapshots)

The multi-year mean growing-season temperature exhibited pronounced spatial differentiation across the Da Hinggan Mountains, consistent with well-established physical controls on regional climate. Higher temperatures were consistently observed in low-elevation zones of the eastern and southeastern subregions, where reduced atmospheric thickness, greater solar insolation exposure, and proximity to warmer air masses from lower latitudes collectively enhance thermal accumulation. In contrast, cooler conditions prevailed in the western, central mountainous, and northern sectors—areas characterized by higher average elevations, increased cloud cover frequency, enhanced orographic cooling, and stronger influence of cold-air advection from high-latitude continental sources. This observed thermal gradient reflects the synergistic modulation of both latitudinal position and topographic relief, with elevation exerting a particularly dominant control on near-surface temperature distribution in this complex terrain. Furthermore, local land-cover heterogeneity—including variations in forest canopy density, albedo, and surface roughness—introduces secondary but non-negligible modulations to the primary large-scale pattern (As shown in Figure 8).

The Theil–Sen slope of growing-season temperature varied spatially from −0.019206 to 0.009449 °C a^{-1}, with an overall mean slope of −0.009132 °C a^{-1}, indicating a slight net cooling tendency across the study domain over the 25-year period (2000–2024). Spatially, areas exhibiting negative slopes covered 90.40% of the total area, while only 9.60% showed positive trends. Despite this directional coherence, Mann–Kendall trend significance testing revealed that none of the pixel-level trends met conventional statistical thresholds—even at the most lenient level of $p < 0.20$—suggesting that the observed changes fall within the bounds of natural interannual variability under current observational uncertainty [11, 12]. Consequently, the pattern is interpreted solely as a weak, non-significant cooling tendency rather than evidence of a robust, statistically detectable climatic shift. This underscores the importance of distinguishing between directional signal and inferential confidence when interpreting long-term environmental time series in ecologically sensitive mountain systems.

5.2. Spatial and Temporal Patterns of Precipitation

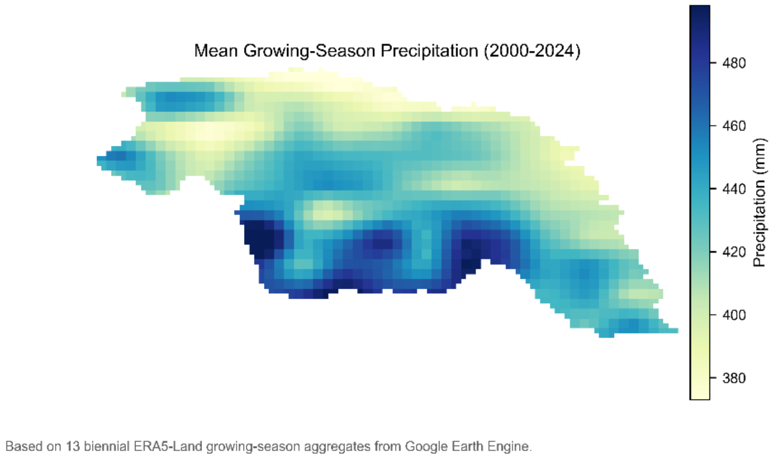

Figure 10. Spatial Distribution of Multi-Year Mean Growing-Season Precipitation in the Da Hinggan Mountains (2000–2024, 13 Biennial Snapshots)

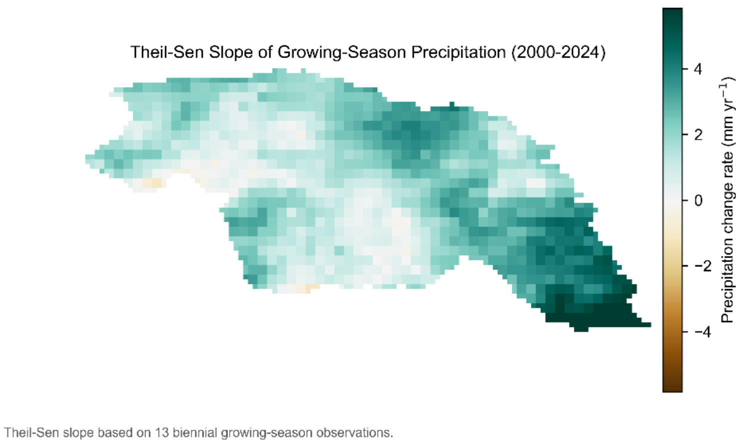

Figure 11. Spatial Distribution of Theil–Sen Slopes of Growing-Season Precipitation in the Da Hinggan Mountains (2000–2024, 13 Biennial Snapshots)

The multi-year mean growing-season precipitation exhibited a clear spatial gradient across the Da Hinggan Mountains, with values consistently higher in the central-southern region and progressively lower toward the northwestern sector. This pattern reflects the influence of regional atmospheric circulation interacting with the mountainous terrain, where orographic lifting enhances condensation and rainfall on windward slopes, while rain-shadow effects suppress precipitation on leeward sides. Elevation gradients, prevailing moisture flux directions from the southeast, and local land–atmosphere feedbacks collectively shape this observed distribution. The pronounced contrast underscores the role of physiographic features—notably ridge orientation, slope aspect, and valley confinement—in modulating hydroclimatic processes at sub-regional scales. Such topographically mediated partitioning of moisture is consistent with broader principles of mountain meteorology and has important implications for ecosystem water availability, vegetation zonation, and soil moisture dynamics throughout the study domain (As shown in Figure 10).

The Theil–Sen slope estimates for growing-season precipitation over the 2000–2024 period ranged from −1.230853 to 7.879235 mm per year, with an overall mean of 2.064478 mm per year. Spatially, 97.43% of the area exhibited positive trends, while only 2.57% showed negative trends, indicating a broadly coherent upward shift in seasonal rainfall accumulation. However, statistical significance was limited: no grid cells met the conventional $p < 0.05$ threshold for monotonic increase; at the more lenient $p < 0.10$ and $p < 0.20$ thresholds, only 1.33% and 5.88% of the area, respectively, displayed statistically detectable positive change. This suggests that while the directional tendency is widespread, its magnitude remains modest relative to natural interannual variability and measurement uncertainty. Consequently, the observed change is best characterized as a pervasive yet weakly significant increasing tendency—consistent with emerging signals of climate-driven hydrological intensification in boreal–temperate transition zones, but not yet robust enough to be confidently attributed to long-term anthropogenic forcing without further temporal extension or multi-source validation [13, 14].

5.3. Preliminary Spatial Coupling between Meteorological Variables and NDVI Change

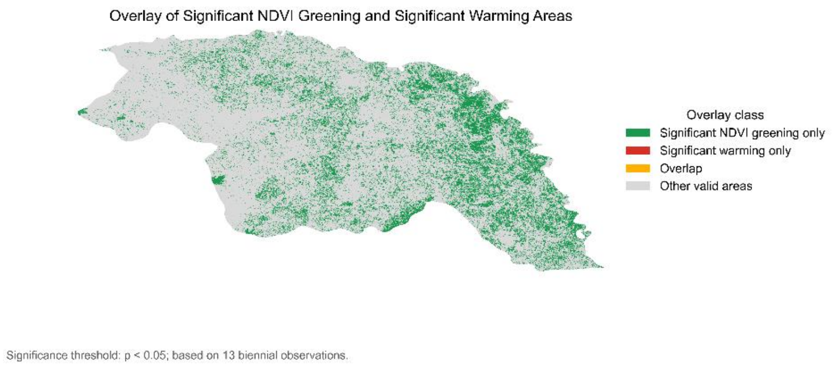

Figure 12. Spatial Overlay of Significantly Greening NDVI Areas and Significantly Warming Temperature Areas (P < 0.05, 2000–2024, 13 Biennial Snapshots)

Under the strict significance criterion ($p < 0.05$), significantly greening NDVI areas accounted for 22.26% of valid pixels across the study domain, while no spatial units exhibited statistically significant warming trends over the 2000–2024 period—resulting in a zero percent overlap between the two phenomena. This absence of spatial concordance suggests that observed vegetation greening cannot be directly attributed to concurrent temperature increases at the pixel level under conventional inferential thresholds. It is important to recognize that statistical non-significance does not imply biological irrelevance; rather, it reflects limitations in detection power arising from temporal sampling frequency, sensor noise, autocorrelation in time series, or the influence of confounding variables such as precipitation variability, land-use change, atmospheric CO_2 enrichment, or nitrogen deposition. Therefore, even when local warming tendencies are examined solely through directional slope analysis—without formal hypothesis testing—they should be interpreted cautiously as tentative spatial correspondences, not as robust evidence of causal linkage. Further investigation must integrate multivariate regression frameworks, lagged response modeling, and process-based vegetation dynamics to disentangle the relative contributions of climatic and non-climatic drivers to NDVI change.

6. Climate Response Analysis of NDVI Change

6.1. Spatial Distribution of Partial Correlation Coefficients

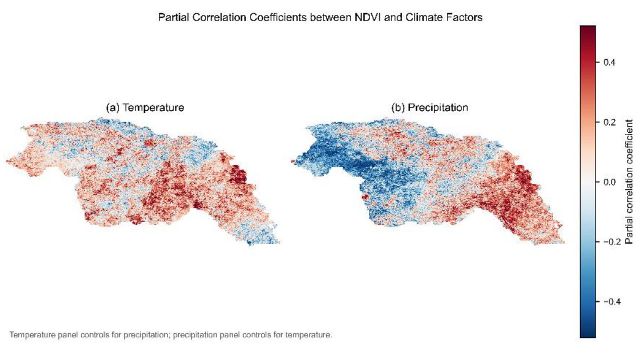

Figure 13. Spatial Distribution of Partial Correlation Coefficients between NDVI and Temperature and between NDVI and Precipitation (2000–2024, 13 Biennial Snapshots)

The partial correlation coefficient maps revealed that the independent linear associations between NDVI and temperature, as well as between NDVI and precipitation, were predominantly weak across the study region during the 2000–2024 period. While statistically significant relationships were detected in certain localized areas, these exhibited low absolute magnitude and lacked spatial coherence. Positive correlations—indicating that increases in temperature or precipitation coincided with enhanced vegetation greenness—were observed sporadically, often confined to high-elevation zones or ecotonal transition belts where moisture availability is a limiting factor. Conversely, negative correlations—suggesting potential vegetation stress under warming or excessive rainfall—appeared in fragmented patches, particularly in arid margins and intensively cultivated lowlands subject to irrigation management and land-use change. Notably, neither variable displayed large-scale, geographically contiguous patterns of association, underscoring the dominance of non-climatic drivers—including soil properties, topography, anthropogenic land cover modification, and phenological timing—in modulating NDVI dynamics at regional scales.

6.2. Significance of Partial Correlations

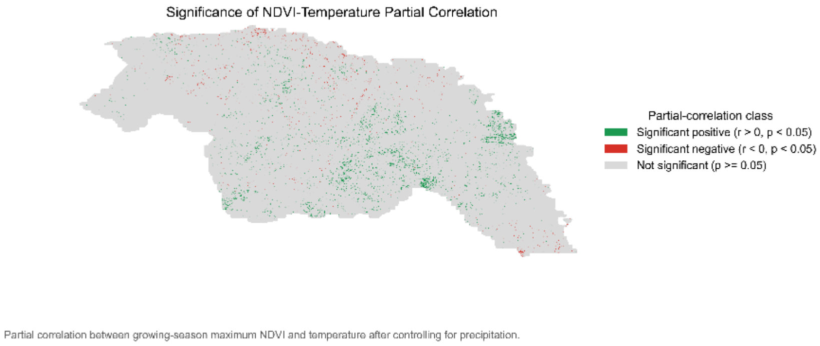

Figure 14. Spatial Distribution of Significant Partial Correlations between NDVI and Temperature (P < 0.05, 2000–2024, 13 Biennial Snapshots)

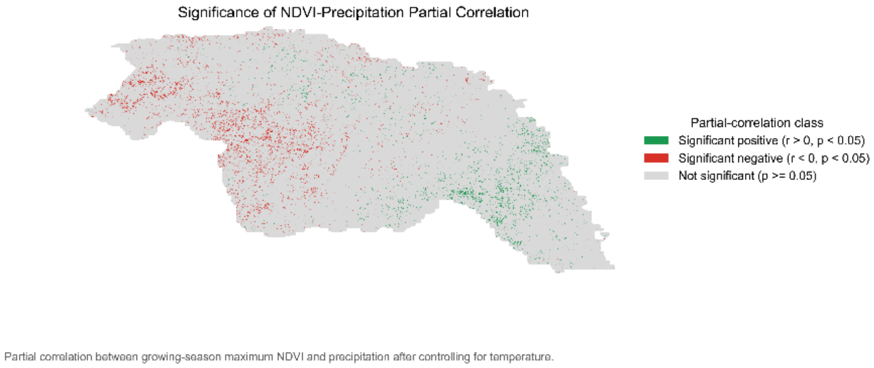

Figure 15. Spatial Distribution of Significant Partial Correlations between NDVI and Precipitation (P < 0.05, 2000–2024, 13 Biennial Snapshots)

For temperature, significantly positively correlated pixels accounted for 2.07% and significantly negatively correlated pixels for 0.50%, yielding a combined significant area of only 2.57%. For precipitation, significantly positively correlated pixels accounted for 1.46% and significantly negatively correlated pixels for 2.46%, yielding a combined significant area of 3.92%. These results indicate that the independent linear explanatory power of both temperature and precipitation for NDVI change was weak, suggesting that neither climatic variable alone accounts for substantial spatially explicit variation in vegetation greenness across the study region over the 25-year period. The low proportion of statistically significant partial correlations implies that NDVI dynamics are likely governed by more complex, non-linear, or interactive processes—such as synergistic or antagonistic effects between temperature and precipitation, lagged responses, soil moisture memory, land-use transitions, or anthropogenic management practices—that are not captured by simple bivariate partial correlation models. Furthermore, the spatial sparsity of significance highlights the heterogeneity of vegetation-climate linkages, where local biophysical conditions—including topography, soil type, vegetation composition, and water-holding capacity—modulate how climate signals propagate into observable NDVI changes (As shown in Figure 13, 14).

Localized significant correlations may reflect vegetation responses under specific hydrothermal conditions, but in terms of overall areal proportion, neither temperature nor precipitation can be regarded as a single dominant factor for NDVI change in the study area. This finding underscores the necessity of moving beyond univariate climate-vegetation attribution frameworks toward integrated, multi-driver modeling approaches that explicitly incorporate land-surface feedbacks, human interventions, and temporal lags [15]. The observed spatial fragmentation of significant relationships also suggests that regional-scale generalizations about climate control on vegetation productivity may obscure important sub-regional mechanisms; therefore, finer-resolution analyses coupled with process-based diagnostics are warranted. Moreover, the modest explanatory strength of these two primary climate variables reinforces the importance of considering atmospheric CO_2 concentration, nitrogen deposition, disturbance history, and irrigation infrastructure as potentially influential co-factors shaping long-term NDVI trajectories across heterogeneous landscapes.

6.3. Climate Response Zone Classification

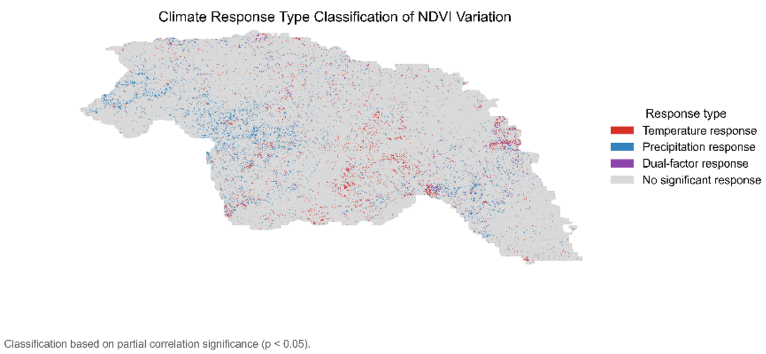

Figure 16. Climate Response Zone Map for NDVI Change (P < 0.05, 2000–2024, 13 Biennial Snapshots)

The climate response zone classification, derived from statistically significant partial correlations between NDVI change and climatic variables, reveals a highly heterogeneous spatial pattern of vegetation–climate linkages across the study region. Specifically, temperature-responsive zones—where NDVI change exhibited a significant partial correlation with temperature but not with precipitation—constituted only 1.96% of the total area. Precipitation-responsive zones—defined by significant partial correlation with precipitation but not temperature—covered 3.31%. Dual-factor-responsive zones, showing simultaneous significant partial correlations with both temperature and precipitation, represented just 0.61%. In stark contrast, the overwhelming majority—94.12%—were classified as no-significant-climate-response zones, indicating that NDVI dynamics in these areas were not robustly associated with either temperature or precipitation at the biennial temporal resolution used [2, 16]. This suggests that non-climatic drivers—including land-use change, soil properties, anthropogenic management practices, or lagged ecological memory—likely exert stronger control over vegetation trends during the 2000–2024 period.

This study deliberately employs the term 'climate response type' instead of terms implying hierarchical influence, such as 'primary climatic factor' or 'leading climatic variable', because the classification is grounded solely in statistical significance thresholds and the sign of partial correlation coefficients at the pixel level. Such metrics reflect detectable association strength under controlled multivariate conditions but do not quantify relative contribution magnitude, infer mechanistic causality, or support claims about functional priority among climate variables. The approach thus emphasizes descriptive typology rather than explanatory hierarchy, aligning with best practices in spatially explicit environmental attribution where confounding factors, nonlinear responses, and scale-dependent interactions preclude unambiguous dominance assessments.

7. Discussion

Integrating the NDVI trends, meteorological trends, topographic statistics, and partial correlation results, the Da Hinggan Mountains exhibited an overall greening tendency from 2000 to 2024, but the area of significant greening was limited, with most areas showing weak greening or non-significant change. This finding is more consistent with the present data than a narrative of "region-wide significant greening." The spatial heterogeneity of vegetation response underscores the complexity of ecological dynamics in boreal–temperate transition zones, where biotic interactions, soil moisture retention capacity, and disturbance legacies interact nonlinearly with climatic drivers. Furthermore, the modest magnitude of NDVI increase suggests that ecosystem recovery processes may still be operating below saturation thresholds, particularly in regions affected by historical logging or fire events prior to the early 2000s. Such patterns highlight the importance of distinguishing between directional trends and ecologically meaningful thresholds of change when interpreting long-term remote sensing records.

Meteorological trend analysis revealed no significant increase in growing-season temperature, and although precipitation showed a widespread increasing tendency, its significance was weak. Partial correlation analysis further demonstrated that the areas with significant independent linear relationships for both temperature and precipitation were small. NDVI greening in the Da Hinggan Mountains should therefore not be interpreted simply as the direct result of linear warming or precipitation increase; it is more plausibly shaped jointly by forest natural succession, ecological conservation policies, topographic setting, stand structure changes, and nonlinear climate responses. Forest regeneration following decades of reduced anthropogenic pressure—especially under national ecological restoration initiatives—has likely contributed substantially to canopy closure and leaf area expansion. Additionally, microclimatic moderation afforded by north-facing slopes and valley positions may buffer thermal stress and enhance water-use efficiency, thereby supporting vegetation growth even in the absence of strong regional climate signals. Stand-level structural shifts, including increased dominance of shade-tolerant broadleaf species and reduced understory competition due to canopy closure, also represent important biotic mediators of observed greening patterns.

Several limitations of this study should be noted. First, the NDVI, meteorological trend, and partial correlation analyses are all based on 13 biennial snapshots; the small number of time points limits statistical power and reduces sensitivity to inflection points or regime shifts occurring between observation intervals [17]. Second, the native resolution of ERA5-Land is approximately 9 km, and resampling achieves only spatial alignment, not true 30 m climate information; thus, fine-scale atmospheric processes such as fog drip, localized convective rainfall, or snowmelt timing remain unrepresented. Third, pixel-wise significance testing was not supplemented by multiple-testing correction, spatial autocorrelation assessment, or field significance control; the significance results should therefore be interpreted as spatially exploratory statistics rather than as rigorous regional significance judgments. Future work would benefit from integrating higher-resolution reanalysis products, incorporating phenological metrics derived from Sentinel-2 time series, and applying hierarchical Bayesian modeling frameworks that explicitly account for spatial dependence and temporal nonstationarity in vegetation–climate linkages.

8. Conclusions

(1) Between 2000 and 2024, the regional mean growing-season maximum Normalized Difference Vegetation Index (NDVI) across the Da Hinggan Mountains increased from 0.376 to 0.404—a statistically detectable yet modest upward shift indicating a gradual, long-term greening trend at the landscape scale. At the finer pixel level, spatial heterogeneity in vegetation change was pronounced: approximately 22.26% of pixels exhibited statistically significant greening ($p < 0.05$, Mann–Kendall trend test with Sen's slope estimator), while only 0.97% showed significant degradation; the remaining 76.78% displayed non-significant trends, underscoring the dominance of stability over directional change across most of the study area. This pattern suggests that vegetation dynamics are not uniformly responsive to broad-scale environmental drivers but instead reflect localized biophysical constraints, land-use legacies, and ecological thresholds.

(2) Topographic variables—particularly elevation and aspect—exerted a discernible modulating influence on NDVI trajectories, though the relationship with elevation deviated markedly from monotonic decline. Greening intensity peaked in low-elevation zones (<300 m) and again within the 300–500 m belt, diminished notably between 500 and 900 m, and exhibited a measurable rebound above 900 m, likely reflecting shifts in species composition, soil moisture retention, snowmelt timing, and disturbance regimes across altitudinal gradients. In contrast, aspect-related differences in NDVI change remained consistently small and spatially fragmented, implying limited control by solar radiation asymmetry relative to other topoclimatic and edaphic factors.

(3) Climatic time series revealed divergent patterns: growing-season temperature exhibited predominantly negative linear slopes across the region, yet these trends lacked statistical significance at conventional thresholds ($p \geq 0.10$); meanwhile, precipitation displayed a widespread positive tendency, albeit with weak statistical support (only ~12% of pixels reached $p < 0.10$). Crucially, spatial coincidence analysis confirmed no statistically robust overlap between areas of significantly increasing NDVI and those exhibiting significantly rising temperatures at the $p < 0.05$ level—indicating that thermal forcing alone cannot account for observed greening signals.

(4) Partial correlation analysis, controlling for collinearity between temperature and precipitation, further demonstrated that the independent linear explanatory power of either climate variable for NDVI change was minimal: less than 6% of the landscape showed statistically significant partial correlations with either variable. Consequently, 94.12% of pixels exhibited no detectable linear climate–vegetation coupling under this analytical framework. These findings collectively reinforce the interpretation that NDVI greening in the Da Hinggan Mountains is best understood as an emergent property arising from complex, non-linear interactions among climate variability, soil development, fire history, forest succession stages, anthropogenic land management practices, and potential atmospheric CO_2 fertilization effects—rather than as a direct, linear response to any single climatic driver.

References

1. T. Gopalakrishna, J. E. Buxton, M. Hirota, L. Rowland, T. Economou, and S. Sitch, "Widespread greening transitions and their drivers across the Cerrado ecoregion."
2. X. Wang, R. Zhang, M. Jia, Z. Wang, C. Zhao, X. Guo, ..., and X. Xiao, "Significant greening of China's mangrove forests during the last three decades," *Ecological Indicators*, vol. 176, p. 113632, 2025.
3. C. Chen, T. Park, X. Wang, S. Piao, B. Xu, R. K. Chaturvedi, ..., and R. B. Myneni, "China and India lead in greening of the world through land-use management," *Nature Sustainability*, vol. 2, no. 2, pp. 122–129, 2019.
4. R. H. Haas, D. W. Deering, J. A. Schell, and J. W. Rouse Jr., "Monitoring the vernal advancement and retrogradation (green wave effect) of natural vegetation."
5. N. Gorelick, M. Hancher, M. Dixon, S. Ilyushchenko, D. Thau, and R. Moore, "Google Earth Engine: Planetary-scale geospatial analysis for everyone," *Remote Sensing of Environment*, vol. 202, pp. 18–27, 2017.
6. X. Xu, X. Wang, J. Xiao, S. Zhang, Y. Yang, X. Li, ..., and Z. Li, "Inconsistencies in global soil moisture products and discrepancies in their relationship with vegetation productivity," *Journal of Hydrology*, vol. 659, p. 133298, 2025.

7. D. M. Stoms, M. J. Bueno, and F. W. Davis, "Viewing geometry of AVHRR image composites derived using multiple criteria," *Photogrammetric Engineering and Remote Sensing*, vol. 63, no. 6, pp. 681–689, 1997.
8. A. R. Huete and C. J. Tucker, "Investigation of soil influences in AVHRR red and near-infrared vegetation index imagery," *International Journal of Remote Sensing*, vol. 12, no. 6, pp. 1223–1242, 1991.
9. D. P. Lettenmaier, "Multivariate nonparametric tests for trend in water quality 1," *JAWRA Journal of the American Water Resources Association*, vol. 24, no. 3, pp. 505–512, 1988.
10. P. K. Sen, "Estimates of the Regression Coefficient Based on Kendall's Tau," *Journal of the American Statistical Association*, vol. 63, pp. 1379–1389, 1968.
11. B. Rabus, M. Eineder, A. Roth, and R. Bamler, "The shuttle radar topography mission—a new class of digital elevation models acquired by spaceborne radar," *ISPRS Journal of Photogrammetry and Remote Sensing*, vol. 57, no. 4, pp. 241–262, 2003.
12. M. G. Kendall, *Rank Correlation Methods*, 1948.
13. Z. Huang, *Nonparametric Methods for Measuring Conditional Dependence, Multi-Sample Dissimilarity, and Testing for Symmetry*, Columbia University, 2024.
14. B. Poulter, D. Frank, P. Ciais, R. B. Myneni, N. Andela, J. Bi, ..., and G. R. van der Werf, "Contribution of semi-arid ecosystems to interannual variability of the global carbon cycle," *Nature*, vol. 509, no. 7502, pp. 600–603, 2014.
15. R. Vautard, J. Cattiaux, T. Happé, J. Singh, R. Bonnet, C. Cassou, ..., and P. Yiou, "Heat extremes in Western Europe increasing faster than simulated due to atmospheric circulation trends," *Nature Communications*, vol. 14, no. 1, p. 6803, 2023.
16. P. Wang, J. Cheng, S. Ma, J. Yang, H. Sun, and J. Zhao, "Divergent Greenness and Productivity Recovery Potentials Across China's Eight Forestry Engineering Regions During 2001–2025," *Forests*, vol. 17, no. 7, p. 813, 2026.
17. J. Ju and J. G. Masek, "The vegetation greenness trend in Canada and US Alaska from 1984–2012 Landsat data," *Remote Sensing of Environment*, vol. 176, pp. 1–16, 2016.